



Local delivery of stabilized chondroitinase ABC degrades chondroitin sulfate proteoglycans in stroke-injured rat brains

Marian H. Hettiaratchi^{a,b}, Matthew J. O'Meara^c, Carter J. Teal^{b,d}, Samantha L. Payne^{a,b,d}, Andrew J. Pickering^a, Molly S. Shoichet^{a,b,d,e,*}

^a Department of Chemical Engineering and Applied Chemistry, University of Toronto, 200 College Street, Toronto, Ontario M5S 3E5, Canada

^b Terrence Donnelly Centre for Cellular and Biomolecular Research, University of Toronto, 160 College Street, Toronto, Ontario M5S 3E1, Canada

^c Department of Pharmaceutical Chemistry, University of California – San Francisco, 1700 Fourth Street, San Francisco, CA 94158-2550, United States

^d Institute of Biomaterials and Biomedical Engineering, 164 College Street, Toronto, Ontario M5S 3G9, Canada

^e Department of Chemistry, University of Toronto, 80 St. George Street, Toronto, Ontario M5S 3H6, Canada

ARTICLE INFO

Keywords:

Chondroitinase ABC
Stroke
PEGylation
Glial scar
Affinity release
Protein delivery
Site-directed mutagenesis
Protein stability
Rosetta

ABSTRACT

Central nervous system (CNS) injuries, such as stroke and spinal cord injuries, result in the formation of a proteoglycan-rich glial scar, which acts as a barrier to axonal regrowth and limits the regenerative capacity of the CNS. Chondroitinase ABC (ChABC) is a potent bacterial enzyme that degrades the chondroitin sulfate proteoglycan (CSPG) component of the glial scar and promotes tissue recovery; however, its use is significantly limited by its inherent instability at physiological temperatures. Here, we demonstrate that ChABC can be stabilized using site-directed mutagenesis and covalent modification with poly(ethylene glycol) chains (*i.e.* PEGylation). Rosetta protein structure modeling was used to screen > 20,000 single point mutations, and four potentially stabilizing mutations were tested *in vitro*. One of the mutations, N1000G (asparagine → glycine at residue 1000), significantly improved the long-term activity of the protein, doubling its functional half-life. PEGylation of this ChABC mutant inhibited unfolding and aggregation and resulted in prolonged bioactivity with a 10-fold increase in activity compared to the unmodified protein after two days. Local, affinity-controlled release of the modified protein (PEG-N1000G-ChABC) was achieved by expressing it as a fusion protein with Src homology 3 (SH3) and delivering the protein from a methylcellulose hydrogel modified with SH3 binding peptides. This affinity-based release strategy provided sustained PEG-N1000G-ChABC-SH3 release over several days *in vitro*. Direct implantation of the hydrogel delivery vehicle containing stabilized PEG-N1000G-ChABC-SH3 onto the rat brain cortex in a sub-acute model of stroke resulted in significantly reduced CSPG levels in the penumbra of 49% at 14 and 40% at 28 days post-injury compared to animals treated with the vehicle alone.

1. Introduction

Chondroitinase ABC (ChABC) is a potent, yet fragile, bacterial enzyme that has generated significant interest as a therapeutic protein due to its ability to degrade perineuronal nets and the proteoglycan-rich component of the glial scar that forms following injury to the central nervous system (CNS), such as after stroke, traumatic brain injury, or spinal cord injury [1,2]. A number of studies have demonstrated improved axonal outgrowth and functional recovery following ChABC treatment, illustrating its ability to overcome the inhibitory nature of glial scar and promote axonal regrowth/remodeling [3–6]. Despite its promise as a therapeutic strategy for CNS repair, use of ChABC is limited by its inherent instability, characterized by rapid protein

aggregation and subsequent loss of activity within several hours at physiological temperature (37 °C) [7,8]. Consequently, ChABC delivery typically requires frequent high-dose bolus injections or continual osmotic pump infusion to ensure sufficient delivery of bioactive enzyme to the injury site [9–11]. While suitable for pre-clinical animal models, this approach increases the risk of infection and exposes surrounding healthy tissue to high levels of the enzyme. Thus, innovations in both the delivery strategy and the long-term activity and stability of ChABC are required.

Methods to stabilize ChABC include modifications to the protein itself (*i.e.* mutagenesis) and co-delivery with stabilizing molecules. Site-directed mutagenesis has been investigated to introduce single point mutations to stabilize flexible regions of the protein [12,13] or

* Corresponding author at: Terrence Donnelly Centre for Cellular & Biomolecular Research, University of Toronto, 160 College Street, Toronto, ON M5S 3E1, Canada.

E-mail address: molly.shoichet@utoronto.ca (M.S. Shoichet).

<https://doi.org/10.1016/j.jconrel.2019.01.033>

Received 13 December 2018; Received in revised form 21 January 2019; Accepted 24 January 2019

Available online 25 January 2019

0168-3659/ © 2019 Elsevier B.V. All rights reserved.

rearrange suboptimal bond angles [14]. Co-delivery with trehalose, sucrose, glycerol, and sorbitol have also demonstrated a protective effect on ChABC activity [15–17]. Surprisingly, covalent modification with stabilizing molecules, such as poly(ethylene glycol) (*i.e.*, PEGylation), has not been investigated with ChABC, perhaps due to the fragility of this enzyme and/or concerns with interference with the catalytic site [18].

Here, we describe a novel two-pronged approach to stabilize ChABC, in which site-directed mutagenesis and PEGylation are used to confer increased protein stability and bioactivity. Rosetta software was used to model the crystal structure of ChABC [19] and predict stabilizing mutations in its amino acid sequence by individually considering the effects of all possible mutations on structural stability. Thus, we demonstrate, for the first time, a rationally designed ChABC mutant with improved bioactivity using a global *in silico* mutagenesis approach. As a parallel strategy, exposed lysine residues on ChABC were PEGylated to further improve protein stability. PEGylation has been shown to prevent protein aggregation and denaturation, extend *in vivo* half-life, and decrease clearance of sensitive proteins [20–24]. Although non-specific PEGylation may interfere with the open catalytic site groove of ChABC, we achieved robust, prolonged enzymatic activity with the conjugation of large (20 kDa), linear PEG chains. The combination of both strategies together (PEGylation and site-directed mutagenesis) resulted in improved ChABC bioactivity and stability, with a 10-fold increase in activity after two days and decreased protein aggregation and unfolding.

To achieve sustained release of this newly stabilized, bioactive ChABC, we expressed ChABC as a fusion protein with the Src homology 3 (SH3) domain (ChABC-SH3), PEGylated the protein, and then distributed the stabilized protein within a methylcellulose hydrogel modified with SH3 binding peptides. Reversible binding interactions between the fusion protein and binding peptides control protein release from the hydrogel [25]. This minimally invasive protein delivery vehicle was injected onto the cortical surface of the brain in a pre-clinical model of stroke, thereby circumventing the blood-brain barrier, and allowing ChABC-SH3 to diffuse into the tissue. We demonstrate that PEG-N1000G-ChABC-SH3 reduces proteoglycan levels in the peri-lesion of the stroke-injured brain at 14 and 28 days post-injury by 49% and 40%, respectively, suggesting that sustained delivery of this stabilized enzyme is a viable strategy for degrading the inhibitory glial scar in stroke and other CNS injuries.

2. Materials and methods

2.1. Materials

Plasmids were purchased from Genscript (Piscataway, NJ). Methoxy-poly(ethylene glycol) succinimidyl valerate (mPEG-SVA; 5, 10, 20 kDa) and biotin-poly(ethylene glycol) succinimidyl valerate (biotin-PEG-SVA; 20 kDa) were purchased from Laysan Bio (Arab, AL). All other materials were purchased from Sigma Aldrich (St. Louis, MO) and used as received unless otherwise specified.

2.2. Rosetta protein structure modeling

Stabilizing mutations were predicted for an apo structure of chondroitinase ABC (ChABC) from *Proteus vulgaris* (Uniprot entry: CABCl_PROVU): chain A of the protein data bank (PDB) entry 1HN0 and solved using x-ray diffraction to a resolution of 1.9 Å [19]. The structure has 1021 residues, with three domains (lyase_N, lyase_catalyt, lyase_8), as identified by Pfam 31.0 [26,27]. The ChABC domains of the fusion protein of ChABC and Src homology 3 (ChABC-SH3) differ from 1HN0 at the termini, missing residues 2–23, containing the amino acids PRVNSPGTRS following residue 1021, and containing the following point mutations: A154T, I309V, L322P, E694P, N738D.

To prepare the structure for design, Rosetta 3 was used to model the

ChABC domains of ChABC-SH3 onto 1HN0 and relaxed the structure in 20 independent trajectories using the FastRelax protocol. This protocol performs 5 rounds of full-atom cartesian-space gradient-based minimization and side-chain rotamer optimization of the ref15 Rosetta energy function [28], while ramping down cartesian, bond angle, and bond length constraints at each round. We then selected the conformation that minimized the energy and all-atom root mean square deviation (RMSD) to the crystal structure. To predict stabilizing mutations, we ran the PmutScan protocol [29], which scans all single-point mutations at all positions separately (> 20,000 mutations) and repacks sidechains around each mutation using the multi-cool annealer, while keeping the backbone fixed. In parallel, we used the ddG protocol [30], which also considers all possible mutations separately, but allows for local backbone and sidechain movement to accommodate the mutation. The change in free energy of folding (ΔG) due to each mutation was evaluated to determine whether the mutation was stabilizing (*i.e.* decrease in free energy) or destabilizing (*i.e.* increase in free energy).

2.3. Chondroitinase ABC-SH3 expression and purification

The fusion protein of chondroitinase ABC and Src homology 3 domain (ChABC-SH3) was expressed and purified as previously described [31]. Briefly, ChABC-SH3 was inserted into a pET28b + vector after the isopropyl β -D-1-thiogalactopyranoside (IPTG)-inducible T7 promoter between existing hexahistidine (HHHHHH) and FLAG (DYKDDDDK) tags, such that the sequence proceeded as follows from the N-terminus to C-terminus: hexahistidine tag, SH3 domain, flexible linker, ChABC, and FLAG tag. Site-directed mutagenesis was performed by ACGT Corporation (Toronto, ON) to introduce the following mutations into the original plasmid based on the 1HN0 crystal structure of ChABC: N1000G, Q140G, T154F, and S431L. Plasmids were transformed into BL21 (DE3) *Escherichia coli* cells (New England Biolabs, Ipswich, MA) for protein expression. Clones were picked from kanamycin-containing Luria Bertani (LB)-agar plates, and transformation with intact plasmids was confirmed *via* Sanger sequencing.

For small-scale verification of protein expression, cells were grown overnight at 37 °C in 10 mL of LB broth supplemented with 50 μ g/mL of kanamycin, followed by induction of protein expression with 0.8 mM IPTG during the log phase of growth ($OD_{600nm} \geq 0.8$) for an additional 5 h. Cell cultures were centrifuged and treated with BugBuster® Protein Extraction Reagent for bacterial lysis. The soluble fraction of the bacterial lysate was denatured in loading buffer and separated by mass using sodium dodecyl sulfate polyacrylamide gel electrophoresis (SDS-PAGE) followed by Coomassie Brilliant Blue staining for non-specific staining of all protein bands.

For large-scale protein production, *E. coli* cells were grown overnight at 37 °C in 20 mL of LB broth supplemented with 50 μ g/ml of kanamycin and then transferred to 1.8 L of Terrific Broth (TB) containing 0.4% glycerol, 50 μ g/mL of kanamycin, and 500 μ L of anti-foaming agent. TB cultures were grown at 37 °C in a LEX-10 bubbler system (Epiphyte3, Toronto, ON) with constant air sparging until $OD_{600nm} \geq 0.8$ was reached, upon which 0.8 mM IPTG was added and protein expression was allowed to proceed at 22 °C overnight. TB cultures were centrifuged for 15 min at 6000 rpm and 4 °C using an Avanti JXN-26 centrifuge (Beckman Coulter, Brea, CA), and the cell pellets were resuspended in 40 mL of lysis buffer (50 mM Tris pH 7.5, 500 mM NaCl, 5 mM imidazole) and lysed using a 500 W sonicator (QSonica, Newtown, CT) at 30% amplitude for 5 min at 10 s intervals. The soluble fraction of the cell lysate was incubated with 1.8 mL of nickel-nitrilotriacetic acid (Ni-NTA) resin for 15 min at 4 °C to promote binding between the nickel resin and hexahistidine tag on ChABC-SH3. The cell lysate was poured through a glass chromatography column, and the Ni-NTA resin was washed with 10 \times 10 mL of wash buffer (50 mM Tris pH 7.5, 500 mM NaCl, 30 mM imidazole) to remove other loosely bound cellular components. Nickel-bound proteins were eluted using a high concentration of imidazole (40 mM Tris pH 7.5, 500 mM NaCl, 250 mM

imidazole), and concentrated to 1–2 mL with a 10,000 kDa cut-off Vivaspin® 20 centrifugal concentrator (Sartorius, Gottingen, Germany). Size exclusion-based purification was performed using fast protein liquid chromatography (Hi-load 16/600 Superdex 200 column, AKTA Purifier 10, GE Healthcare Life Sciences, Budapest, Hungary) in 50 mM sodium acetate in phosphate-buffered saline (PBS) (pH 8.0). Purified ChABC-SH3 was filter-sterilized (Amicon Ultrafree-MC 0.22 µm Centrifugal Filter Units, Millipore Sigma, Burlington, MA) and stored in 50 mM sodium acetate in PBS (pH 8.0) at –80 °C until use.

2.4. Chondroitinase ABC-SH3 activity

The enzymatic activity of ChABC-SH3 was evaluated by measuring the degradation of the substrate chondroitin sulfate A, which exhibits an absorbance change at 232 nm following ChABC-SH3 digestion. 10 µL of 0.1 mg/mL ChABC-SH3 was mixed with 90 µL of 10 mg/mL chondroitin sulfate A in a UV-Star® microplate (Greiner Bio-One, Monroe, NC) and immediately read on a plate reader (Tecan Infinite M200 Pro) at 232 nm. Readings were taken at room temperature every 20 s for 20 min, and the slope of the resultant linear relationship between absorbance and time was used to calculate the kinetic activity of ChABC-SH3 in units of activity (mmol substrate degraded per min) per mg of protein (U/mg).

To evaluate long-term enzymatic activity, solutions of 0.1 mg/mL of ChABC-SH3 in PBS (pH 7.4) with 0.1% (w/v) bovine serum albumin (BSA) and protease inhibitors (cOmplete Mini, EDTA-free Protease Inhibitor Cocktail, Roche, Basel, Switzerland) were incubated at 37 °C for 0–48 h; samples were frozen at –80 °C until analysis. The half-life of active ChABC-SH3 was calculated by fitting activity data over time to a one-phase exponential decay curve. The total potential for substrate degradation was determined by calculating the area under the curve (AUC) of the ChABC-SH3 activity data over time using the trapezoid rule.

2.5. Circular dichroism

Far-UV circular dichroism (CD) spectra were measured between 200 and 260 nm (average of three spectra) using a JASCO J-810 CD spectrophotometer (JASCO, Easton, MD). All results were expressed as molar ellipticity ($\text{deg cm}^2 \text{dmol}^{-1}$). ChABC-SH3, mutants, PEGylated ChABC-SH3 (PEG-ChABC-SH3), and ChABC-SH3 mixed with free 20 kDa PEG were diluted to 0.2 mg/mL in PBS (pH 7.4) and pipetted into a glass cuvette with a 1 cm path length. Proteins were first analyzed at room temperature from 200 to 260 nm, and the CD spectra were used to determine α -helix and β -sheet content *via* deconvolution on Dichroweb [32] (University of London, United Kingdom). Thermal denaturation resulting in protein unfolding and loss of secondary structure was performed using a 1 °C/min temperature scan between 25 and 70 °C at a single wavelength (217 nm). Melting temperatures (T_m) were determined using Boltzmann regression for the midpoint of the linear denaturation curve.

2.6. Static light scattering

Static light scattering (SLS) measurements were performed using a UNit instrument (Unchained Labs, Pleasanton, CA). Proteins were diluted to 1 mg/mL in PBS (pH 7.4) and pipetted into 9 µL glass capillaries. SLS readings at 466 nm were taken between 25 and 70 °C using a temperature scan rate of 1 °C/min to evaluate protein unfolding and subsequent aggregation. Melting temperatures (T_m) were determined using Boltzmann regression for the midpoint of the linear denaturation curve. SLS at 466 nm was also measured during isothermal incubation at 37 °C for 4 h.

2.7. Poly(ethylene glycol) modification of chondroitinase ABC-SH3

ChABC-SH3 was covalently modified with methoxy-poly(ethylene glycol) succinimidyl valerate (mPEG-SVA) or biotin-poly(ethylene glycol) succinimidyl valerate (biotin-PEG-SVA), which form amide bonds with the primary amines (*i.e.* lysines) on proteins. 69 partially exposed lysines (66 in ChABC, 3 in SH3) were available for PEGylation (Fig. 4A). mPEG-SVA (5, 10, 20 kDa) or biotin-PEG-SVA (20 kDa) was dissolved in 50 mM sodium acetate in PBS (pH 8.0) at 5 mg/mL and added to 1 mg/mL of ChABC-SH3 in 1–100 times molar excess mPEG-SVA to protein. The reaction was allowed to proceed for 1 h at room temperature with gentle agitation before excess mPEG-SVA or biotin-PEG-SVA was removed using a 50 kDa cut off Amicon-Ultra Centrifugal Filter spin column (MilliporeSigma). 1 mg/mL ChABC-SH3 was also incubated with 100 times molar excess PEG (with no reactive groups) as a control.

Unmodified ChABC-SH3 and ChABC-SH3 modified with different amounts of 20 kDa mPEG-SVA were run on an SDS-PAGE gel and stained with Coomassie Brilliant Blue to evaluate the change in molecular weight due to PEGylation. To determine the average number of PEG chains attached to ChABC-SH3 using different reaction conditions (1–100 times molar excess), biotin content of ChABC-SH3 modified with 20 kDa biotin-PEG-SVA was analyzed using a Pierce™ Biotin Quantification Kit (Thermo Fisher Scientific, Mississauga, ON, Canada) and normalized to the same initial concentration of free biotin-PEG-SVA run through a 50 kDa cut off spin column.

2.8. Fabrication of methylcellulose hydrogel

5% (w/v) chemically cross-linked methylcellulose (MC) hydrogels were fabricated as previously described [33]. All materials were sterile-filtered through a 0.22 µm filter prior to use. Briefly, the hydroxyl groups of 300 kDa methylcellulose (Shin Etsu, Tokyo, Japan) were modified with reactive thiols (MC-SH) or a binding peptide for the SH3 domain (KPPVVKKPHYLS) with an approximate dissociation constant (K_D) of 2.7×10^{-5} M (MC-peptide) [31]. MC-SH, MC-peptide, and unmodified MC were mixed to obtain a 1:100 ratio of protein to binding peptides and 0.1 µmol thiol per 100 µL of hydrogel with a final concentration of 5% (w/v) methylcellulose in artificial cerebrospinal fluid (aCSF; 149 mM NaCl, 3 mM KCl, 0.8 mM MgCl₂, 1.4 mM CaCl₂, 1.5 mM Na₂HPO₄, 0.2 mM NaH₂PO₄ at pH 7.4). Repeated rounds of speed-mixing (35,000-g, 1 min) using a SpeedMixer DAC 150 FV2 (FlackTek, Landrum, SC) and centrifugation (12,000-g, 30 s) were used to dissolve the polymers. ChABC-SH3 was speed-mixed into the dissolved MC polymer solution at 200 µg/mL of hydrogel for *in vitro* protein release experiments and 1.67 mg/mL of hydrogel for *in vivo* implantation in the rat stroke model. The MC-SH was chemically cross-linked using a 3000 Da PEG-bismaleimide cross-linker (Rapp Polymere, Tuebingen, Germany) at a molar ratio of 0.75:1 maleimide to thiol and allowed to form a hydrogel overnight at 4 °C prior to use.

2.9. *In vitro* chondroitinase ABC-SH3 release from methylcellulose hydrogels

Cross-linked methylcellulose hydrogels containing one of the following: (1) binding peptide + ChABC-SH3, (2) binding peptide + PEGylated ChABC-SH3 with the N1000G mutation (*i.e.* PEG-N1000G-ChABC-SH3), (3) no binding peptide + PEG-N1000G-ChABC-SH3, or (4) no protein were loaded into 500 µL Hamilton syringes. 100 µL of hydrogel were injected through an 18-gauge needle into a 2 mL microcentrifuge tube (Axygen® Maxymum Recovery™) and centrifuged to create a flat surface. 400 µL of aCSF were immediately added to each hydrogel, and the tubes were incubated at 37 °C with gentle agitation. aCSF was carefully removed and replaced at 0 h, 2 h, 6 h, and 1, 2, 4, and 7 d. Release of ChABC-SH3 and PEG-N1000G-ChABC-SH3 was quantified using an enzyme-linked immunosorbent assay (ELISA) for

the hexahistidine and FLAG tags as previously described [22], compared to a standard curve of known ChABC-SH3 and PEG-N1000G-ChABC-SH3 concentrations, and normalized to aCSF incubated with blank hydrogels for the same amount of time.

2.10. Approval for animal work

All surgical procedures were conducted according to the Guide to the Care and Use of Experimental Animals (Canadian Council on Animal Care) and approved by the Animal Care Committee at the University of Toronto. A total of 41 8-week-old male Sprague Dawley rats (between 200 and 250 g) (Charles River, QC, Canada) were used in these studies.

2.11. Endothelin-1 stroke model and hydrogel delivery

Stroke surgeries were performed as previously described [34]. Briefly, male Sprague Dawley rats (200–250 g) were anesthetized with 5% isoflurane, their heads were shaved and cleaned, and placed into a Kopf stereotaxic instrument. An off-midline incision was made in the scalp, and a 2.7 mm burr hole, centered at AP +1.15 mm and ML +3.0 mm, was made in the right hemisphere using a trephine drill bit (Cat. 18,004-27, Fine Science Tools Inc., Vancouver, BC, Canada). To induce a stroke injury, 1 μ L of 400 pmol/ μ L endothelin-1 (Et-1) solution (Calbiochem, San Diego, CA) was injected into three locations in the brain at 0.25 μ L/min using an automated microinjector (Harvard Apparatus, Saint-Laurent, QC, Canada) and a 10 μ L Hamilton syringe fitted with a 26-gauge needle (Model 1701 RN, Hamilton). Et-1 injections were made into the following coordinates relative to bregma in the motor cortex and striatum: (1) anteroposterior (AP) 0.0 mm, mediolateral (ML) +3.0 mm, dorsoventral (DV) -2.3 mm; (2) AP +2.3 mm, ML +3.0 mm, DV -2.3 mm; and (3) AP +0.7 mm, ML +3.8 mm, DV -7.0 mm. Following injection, we waited 2 min prior to withdrawing the needle to prevent Et-1 backflow. After completion of the three injections, a medical grade sterile silicone sheet (2.5-mm in diameter, Bio-Plexus, Ventura, CA) was placed on the exposed dura surface of the brain and the cranial defect was filled with gelfoam (Spongostan Standard, MS0002, Ethicon, New Jersey, USA). The defect was then sealed with bone cement (Ortho-Jet BCA, Lang Dental, Illinois, USA), and the skin was sutured closed.

Seven days post-surgery, hydrogels were implanted onto the surface of the brain as previously described [34]. A second incision was made in the skull, and the previously applied bone cement sealant, gelfoam, and silicone sheet were removed. The dura was then surgically resected with the aid of a surgical microscope, and a 5.9-mm diameter curved sterile polycarbonate disc with a 2.7-mm diameter hole was fixed with bone glue (Henkel Corporation, Rocky Hill, CT) onto the skull over the previously drilled burr hole. 6 μ L of cross-linked methylcellulose hydrogel containing 0.3 U (~10 μ g) of ChABC-SH3, PEG-N1000G-ChABC-SH3, or no protein (vehicle control) was carefully injected into the hole in the polycarbonate disc using an 18-gauge needle, so that the hydrogel was in contact with the cortical surface of the brain and filled the space formed by the skull and polycarbonate disk. A second 5.9-mm diameter sterile polycarbonate disc (without a hole) was placed on top of the hydrogel and secured with Ortho-Jet™ BCA dental cement (Lang Dental, Wheeling, IL, USA).

2.12. Brain tissue processing and staining

Animals were sacrificed at 9, 14, or 28 d post-stroke. Each animal was perfused transcardially with 100 mL of cold PBS followed by 100 mL of 4% paraformaldehyde (PFA) prior to dissection. Dissected brains were incubated in 4% PFA overnight at 4 °C, followed by cryoprotection in 15% sucrose for 1 day, then 30% sucrose until tissue was saturated with sucrose. Brains were frozen in dry ice and 2-methylbutane, and cut into 25 μ m coronal serial sections using a cryostat

(Leica, Buffalo Grove, IL). Every tenth section was stained and analyzed.

Sections were stained for cell nuclei using DAPI (1 μ g/mL; Invitrogen 62,248), mature neurons using rabbit anti-NeuN antibody (1:500; Abcam ab177587), and chondroitin sulfate proteoglycans (CSPGs) using mouse anti-chondroitin sulfate (CS56) antibody (1:100; Sigma Aldrich SAB4200696). Sections were permeabilized for 15 min in 1% (v/v) Triton X-100 in PBS at room temperature, washed three times for 5 min with PBS, blocked for 1 h in 0.1% (v/v) Triton X-100 and 5% (w/v) BSA in PBS, and incubated with primary antibodies in blocking solution overnight at 4 °C. The next day, sections were washed three times for 5 min in PBS, incubated with DAPI, goat anti-rabbit IgG Alexa Fluor 546 (Invitrogen), and goat anti-mouse IgG Alexa Fluor 488 (Invitrogen) fluorescent secondary antibodies (1:500) for 1 h, washed in PBS again, and mounted with ProLong® Gold Antifade Mounting Medium (Thermo Fisher Scientific).

2.13. Brain tissue imaging and analysis

Sections were imaged using an AxioScan.Z1 slide scanner (Zeiss, Oberkochen, Germany) at 10 \times magnification. A custom MATLAB (Mathworks, Natick, MA) program was created for image analysis. Images were split into red, green, and blue channels corresponding to NeuN, CS56, and DAPI staining, respectively. Red (NeuN) and blue (DAPI) channels were merged to create a new image. The stroke lesion was defined as DAPI⁺/NeuN⁻. A region of interest (ROI) was drawn around the lesion [35], discounting the corpus callosum, which naturally lacks neurons. The total lesion volume was calculated by multiplying the lesion area on each section by the distance between sections. Additional areas of interest were created at a distance of 100 and 200 μ m away from the lesion border and were defined as peri-lesional regions. A circular structuring element with a diameter corresponding to the defined peri-lesional distance (100 μ m and 200 μ m) was passed over each of the pixels in the ROI to create a dilated ROI, and each pixel within the area was set to a value of 1 or 0 depending on the presence or absence of signal. The dilated ROI was subtracted from the original ROI to yield the peri-lesional region. The Otsu thresholding algorithm [36] was used to remove any staining artifacts from the ROI and peri-lesional regions based on DAPI staining. The Moments thresholding algorithm [37] was then applied to the green channel to identify CS56 staining. The number of CS56⁺ pixels in the ROI and peri-lesion, as well as the total area of ROI and peri-lesional regions were quantified in each image. The average percentage of CS56⁺ pixels in each brain was calculated based on the total number of sections quantified.

2.14. Statistical analysis

All data are reported as mean \pm standard error of the mean (SEM). *In vitro* experiments were performed with a minimum of 3 replicates for each experimental group. *In vivo* stroke surgeries were performed on 4–5 animals per group per time point. Statistical significance was determined using one-way or two-way ANOVA as appropriate, followed by Tukey's *post hoc* analysis (Graphpad Prism, Version 7.0, La Jolla, CA). $p < .05$ was considered statistically significant. One-phase exponential decay curve fitting, Boltzmann regressions, and area under the curve analyses were also performed using Graphpad Prism.

3. Results

3.1. Prediction of stabilizing point mutations by Rosetta

Using Rosetta, > 20,000 point mutations in the ChABC amino acid sequence were screened computationally using rigid and flexible backbone protocols (PMutScan and ddG) to identify mutations that could potentially stabilize the protein structure. We evaluated each candidate mutation with favorable predicted free energy of mutation

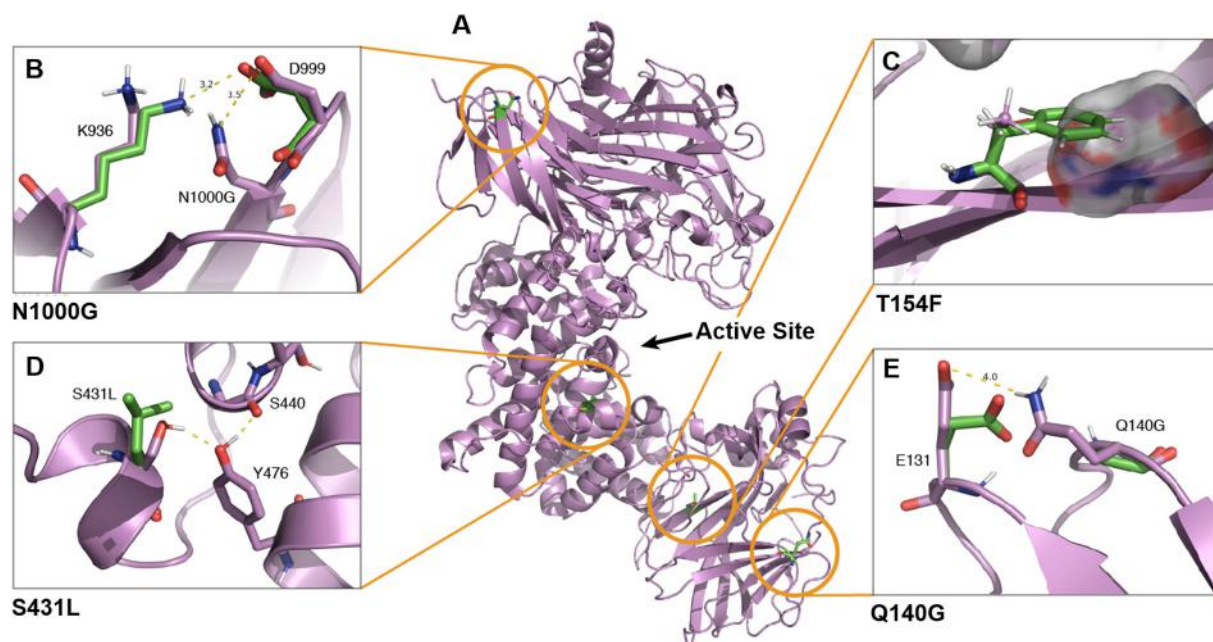


Fig. 1. Stabilizing point mutations in chondroitinase ABC sequence predicted by Rosetta. A) Crystal structure of ChABC with point mutations and active site labeled. B) N1000G (asparagine to glycine at position 1000) mutation. C) T154F (threonine to phenylalanine at position 154) mutation. D) S431L (serine to lysine at position 431) mutation. E) Q140G (glutamine to glycine at position 140) mutation. Native residues are shown in purple, and mutated residues in green. Each panel B-E depicts the optimal conformation after relaxing the backbone and side-chains in the neighborhood of the candidate residues with and without the mutation. Panel C also shows the cavity adjacent to T154 filled by phenylalanine. In individual amino acids, blue represents nitrogen, red represents oxygen, and gray represents hydrogen. Rendering was done with PyMOL [39]. (For interpretation of the references to colour in this figure legend, the reader is referred to the web version of this article.)

Table 1

List of experimentally tested ChABC-SH3 point mutations predicted by Rosetta.

Mutation	Predicted $\Delta\Delta G$ (kcal/mol)	Rosetta protocol
N1000G	−12.4	PMutScan
Q140G	−6.4	PMutScan
T154F	−9.9	ddG
S431L	−7.4	ddG

for burial, participation in critical structural features including capping motifs, proximity to unstructured regions or the active site [38], or relation to mutations present in ChABC-SH3. Based on these criteria, the following mutations were chosen for protein expression and further experimental evaluation: N1000G, Q140G, T154F, and S431L (Fig. 1A, Table 1). The fixed backbone PMutScan protocol predicted a total of 26 stabilizing mutations using a free energy of mutation threshold ($\Delta\Delta G$) of -10 kcal/mol. Of these, we selected N1000G (asparagine to glycine) for further investigation. In the wild-type protein, N1000 folds back and forms a poor hydrogen bond with D999. Mutating this asparagine residue to glycine removes this interaction, allowing N936 to form a more stable hydrogen bond with D999 (Fig. 1B, Supplementary Fig. S1). The flexible backbone ddG protocol yielded 5 mutations with a predicted change in free energy ($\Delta\Delta G$) that was less than -10 kcal/mol and 100 mutations with a predicted change in free energy that was less than -5 kcal/mol. We selected the mutation T154F (threonine to phenylalanine), which was mutated in ChABC-SH3 compared to the x-ray crystal structure (1HN0) as A154T. Placing the bulky phenylalanine on the β -sheet at residue 154 fills a buried cavity better than the smaller alanine or threonine (Fig. 1C, Supplementary Fig. S2). The ddG protocol predicted increased stability with larger residues including tyrosine (-8.2 kcal/mol), phenylalanine (-9.9 kcal/mol), and tryptophan (-13.2 ddG kcal/mol). We also selected mutation S431L (serine to lysine), which is one of two adjacent serine residues on a partially buried, short broken helix (ddG protocol: -7.4 kcal/mol). Both the PMutScan and ddG protocols predicted stabilizing mutations for S431

to non-polar residues, decreasing the desolvation penalty, and removing an out-of-plane hydrogen bond to Y476 (Fig. 1D, Supplementary Fig. S3). Finally, we also considered mutation Q140G (glutamine to glycine), which has been previously tested [13], and was predicted to result in a more modest free energy change using both protocols (ddG protocol: -4.2 kcal/mol; PMutScan: -6.43 kcal/mol) (Fig. 1E, Supplementary Fig. S4).

3.2. Stability and activity of chondroitinase ABC-SH3 mutants

All SH3 fusion protein variants (ChABC-SH3, N1000G, Q140G, T154F, S431L) were successfully expressed in BL21 (DE3) *E. coli* (Fig. S5). ChABC-SH3, N1000G-ChABC-SH3, and Q140G-ChABC-SH3 exhibited similar initial levels of activity based on their ability to degrade chondroitin sulfate A; however, T154F and S431L mutations resulted in almost complete loss of activity (Fig. 2A). Investigation into the long-term activity of these proteins at a physiological temperature of 37°C and pH 7.4 revealed gradual loss of activity in all variants over 24 h. The N1000G mutation exhibited higher activity than ChABC-SH3 at 7, 12, and 24 h, while the Q140G mutation exhibited lower activity than ChABC-SH3 at 2 and 4 h, and similar activity at all other time points. When the change in activity of each protein was fit to a one-phase exponential decay curve, the resultant half-life of N1000G-ChABC-SH3 was double that of ChABC-SH3 and significantly higher than all other mutants (Fig. 2B). Similarly, the area under the curve (AUC) and total potential for substrate degradation was highest with the N1000G mutation compared to all other proteins (Fig. 2C). Large-scale (1.8 L) culture of ChABC-SH3 variants resulted in the production of several milligrams of protein, with the N1000G-ChABC-SH3 variant yielding significantly more protein than the original sequence (Fig. 2D).

To provide further insight into the differences observed in ChABC-SH3 activity, we investigated the effects of the four point mutations on ChABC-SH3 structure and stability, as measured by protein unfolding and aggregation. Far-UV circular dichroism spectra of ChABC-SH3 variants revealed similar α -helix and β -sheet content between proteins

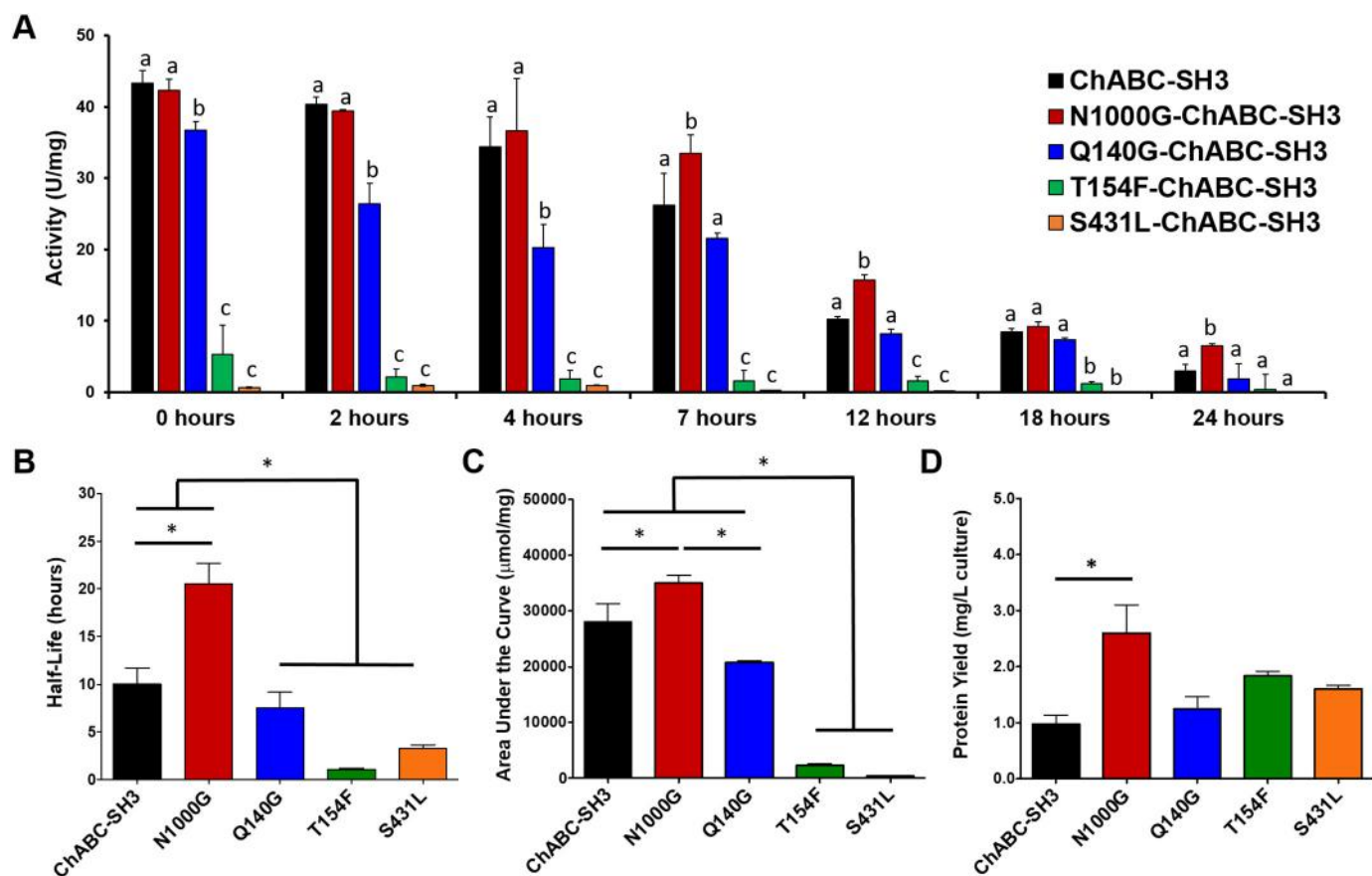


Fig. 2. Activity of ChABC-SH3 is affected by point mutations. A) Specific activity of ChABC-SH3 and mutants after incubation at 37 °C in 0.1% BSA in PBS (pH 7.4) for 0, 2, 4, 7, 12, 18, and 24 h. (At each time point, only bars with different letters are statistically different.) B) Half-life of ChABC-SH3 and mutated ChABC-SH3 based on specific activity. C) Area under the curve (AUC) or total potential substrate degraded by ChABC-SH3 and mutated ChABC-SH3 over 24 h. D) ChABC-SH3 and mutant yield from large volume (1.8 L) *E. coli* cultures. ($n = 3$, mean \pm SEM, * $p < .05$).

(Fig. 3A, Table 2). Furthermore, thermal denaturation curves obtained using circular dichroism (CD) and static light scattering (SLS) both demonstrated similar rates of protein unfolding regardless of mutation, within a narrow range of melting temperatures (T_m) between 48 and 50 °C (Fig. 3B, C, Table 2). Consequently, the investigated point mutations did not result in significant changes to the structural stability of ChABC-SH3 and could not readily explain the observed changes in ChABC-SH3 activity.

Table 2

Structural parameters (α -helix and β -sheet content) and melting temperatures of ChABC-SH3 variants as determined by circular dichroism (CD) and static light scattering (SLS).

Protein	α -Helix (%)	β -Sheet (%)	T_m by CD (°C)	T_m by SLS (°C)
ChABC-SH3	38	20	48	49
N1000G-	39	20	49	48
Q140G-	35	22	49	49
T154F-	33	20	49	50
S431L-	34	25	50	50

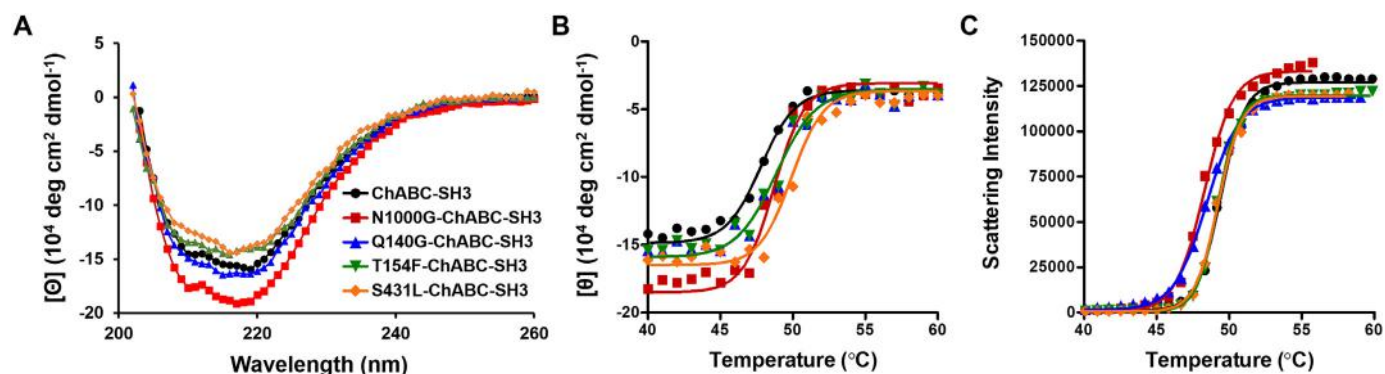


Fig. 3. Point mutations result in similar ChABC-SH3 stability. A) Circular dichroism spectra from 200 to 260 nm at 25 °C. B) Thermal denaturation curves over 40–60 °C (1 °C/min temperature increase) measured by circular dichroism at 217 nm. C) Thermal denaturation curves over 40–60 °C (1 °C/min temperature increase) measured by scattering intensity of solution.

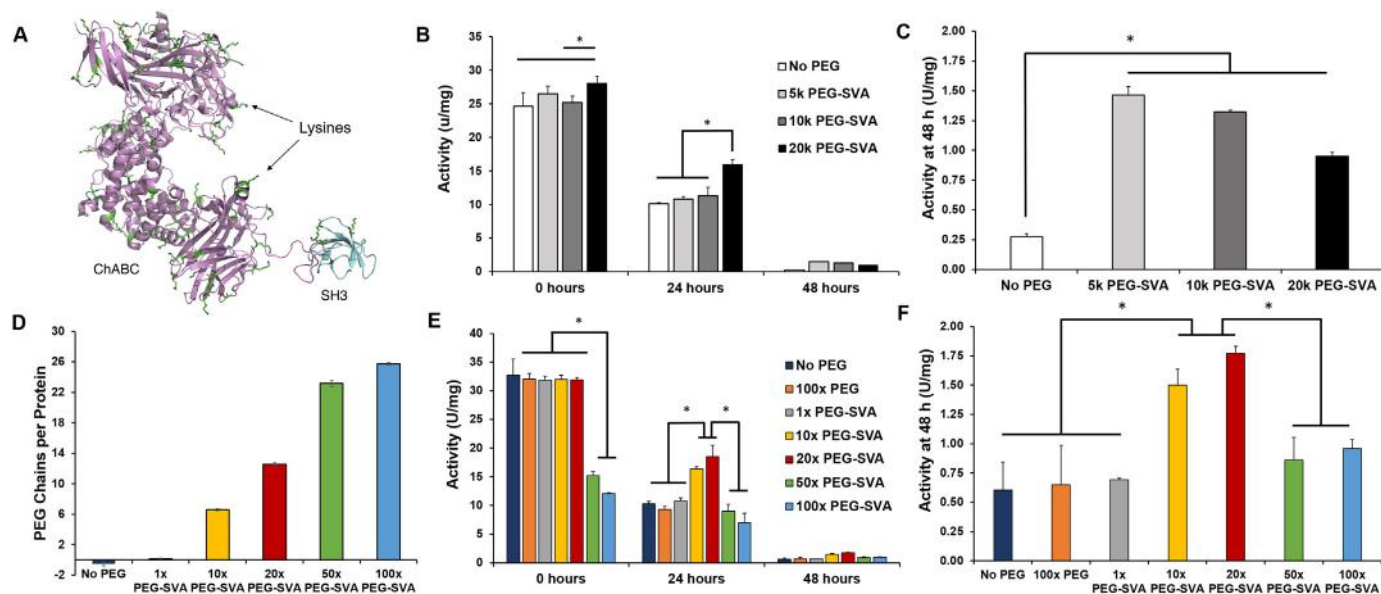


Fig. 4. PEGylation affects ChABC-SH3 activity. A) Structure of ChABC-SH3 with lysines available for PEGylation with mPEG-SVA labeled in green. B) ChABC-SH3 was reacted with 5 kDa, 10 kDa, and 20 kDa mPEG-SVA at 10 times molar excess to protein. Specific activity of ChABC-SH3 and PEGylated ChABC-SH3 after incubation in 0.1% BSA in PBS (pH 7.4) at 37 °C for 0, 24, and 48 h. C) Specific activity of ChABC-SH3 and PEGylated ChABC-SH3 after incubation at 37 °C for 48 h. D) ChABC-SH3 was reacted with 20 kDa biotin-PEG-SVA at 1, 5, 10, 50, and 100 times molar excess of PEG to protein. Quantification of average number of PEGs per protein was based on biotin detection. E) ChABC-SH3 was reacted with 20 kDa mPEG-SVA at 1, 5, 10, 50, and 100 times molar excess to protein, as well as 20 kDa non-functionalized PEG at 100 times molar excess to protein. Specific activity of ChABC-SH3 and PEGylated ChABC-SH3 after incubation in 0.1% BSA in PBS at 37 °C for 0, 24, and 48 h. F) Specific activity of ChABC-SH3 and PEGylated ChABC-SH3 after incubation at 37 °C for 48 h. ($n = 3$, mean \pm SEM, * $p < .05$). (For interpretation of the references to colour in this figure legend, the reader is referred to the web version of this article.)

3.3. Stability and activity of PEGylated chondroitinase ABC-SH3

Although we successfully enhanced the bioactivity of ChABC-SH3 through site-directed mutagenesis, we wondered whether its activity could be further prolonged through additional stabilization strategies. We applied a second approach to stabilizing ChABC-SH3 by covalently conjugating poly(ethylene glycol) (PEG) chains to its lysine residues using methoxy-poly(ethylene glycol) succinimidyl valerate (mPEG-SVA). ChABC-SH3 contains 69 partially exposed lysines, which are available for PEGylation (Fig. 4A). Three different sizes of mPEG-SVA (5, 10, and 20 kDa) were reacted with ChABC-SH3 at 10 times molar excess PEG to protein and purified using a 50 kDa molecular weight cut off spin column. Attachment of 20 kDa mPEG-SVA increased the initial activity of the protein and activity after 24 h of incubation at 37 °C (Fig. 4B). All PEG chains (5, 10, 20 kDa) significantly increased ChABC-SH3 activity after 48 h compared to the unmodified protein (Fig. 4C).

Since conjugation of 20 kDa mPEG-SVA improved ChABC-SH3 activity the most, we further optimized the conjugation conditions by incubating ChABC-SH3 with 1–100 times molar excess mPEG-SVA to protein. PEGylation of ChABC-SH3 with increasing amounts of mPEG-SVA resulted in a stepwise increase in molar mass of the protein as visualized through SDS-PAGE (Fig. S6). At the highest excess of mPEG-SVA (50 and 100 times), the mass of the protein inhibited its penetration into the separating gel. Use of biotin-PEG-SVA enabled quantification of the average number of PEG chains bound to ChABC-SH3 via biotin detection. Reaction with 1, 10, 20, 50, or 100 times molar excess biotin-PEG-SVA to protein resulted in an average of 0.2 ± 0.1 , 6.6 ± 0.2 , 12.6 ± 0.4 , 23.2 ± 0.2 , and 25.7 ± 0.1 PEG chains per protein, respectively (Fig. 4D). Protein PEGylated with 50 and 100 times molar excess mPEG-SVA exhibited significantly reduced initial enzymatic activity (Fig. 4E), likely due to steric hindrance of the enzyme's catalytic site. Reaction conditions using 10 and 20 times excess mPEG-SVA significantly increased ChABC-SH3 activity at 24 and 48 h compared to the unmodified protein and all other PEGylated proteins (Fig. 4E, F). PEGylation reactions containing 1, 50 and 100 times excess

PEG to protein did not significantly change long-term ChABC-SH3 activity (at 24 and 48 h). Moreover, the simple addition of 100 times excess of non-functionalized PEG did not impact ChABC-SH3 activity at any time point, indicating that covalent conjugation of PEG was necessary to preserve activity. Since reaction conditions containing both 10 and 20 times excess of 20 kDa mPEG-SVA improved long-term ChABC-SH3 activity with no difference between the performance of the two, we chose to move forward with the lower degree of ChABC-SH3 modification.

Next, we investigated the effect of PEGylation on ChABC-SH3 structure and stability using CD and SLS. ChABC-SH3 mixed with 10 times excess of free non-functionalized PEG (ChABC-SH3 + PEG) was included as an additional control. Far-UV CD spectra of ChABC-SH3, PEG-ChABC-SH3, and ChABC-SH3 + PEG at room temperature were similar and did not demonstrate any significant shifts with PEGylation (Fig. 5A). Interestingly, both CD and SLS thermal denaturation curves revealed that PEGylation of ChABC-SH3 completely inhibited protein denaturation, while unmodified ChABC-SH3 and ChABC-SH3 + free PEG resulted in rapid, characteristic protein denaturation (Fig. 5B, C). Since CD directly measures protein unfolding and SLS measures protein aggregation by increase in average particle diameter, these results demonstrate that PEGylation inhibited both protein unfolding and aggregation concurrently and further confirmed the need for covalent attachment of PEG chains for an observable effect on ChABC-SH3 stability. Additionally, while ChABC-SH3 and ChABC-SH3 + PEG samples removed from the CD spectrophotometer after thermal denaturation exhibited large protein aggregates visible to the naked eye, PEG-ChABC-SH3 samples did not. To determine whether PEGylation could inhibit protein aggregation under physiologically relevant conditions, proteins were also incubated in the UNit instrument at 37 °C for 4 h and SLS measurements were taken periodically. ChABC-SH3 and ChABC-SH3 + PEG demonstrated a gradual increase in scattering, indicative of the slow formation of protein aggregates, while the scattering intensity of PEGylated ChABC-SH3 did not change (Fig. 5D). These data indicate that PEGylation contributed to ChABC-SH3 stability and activity largely

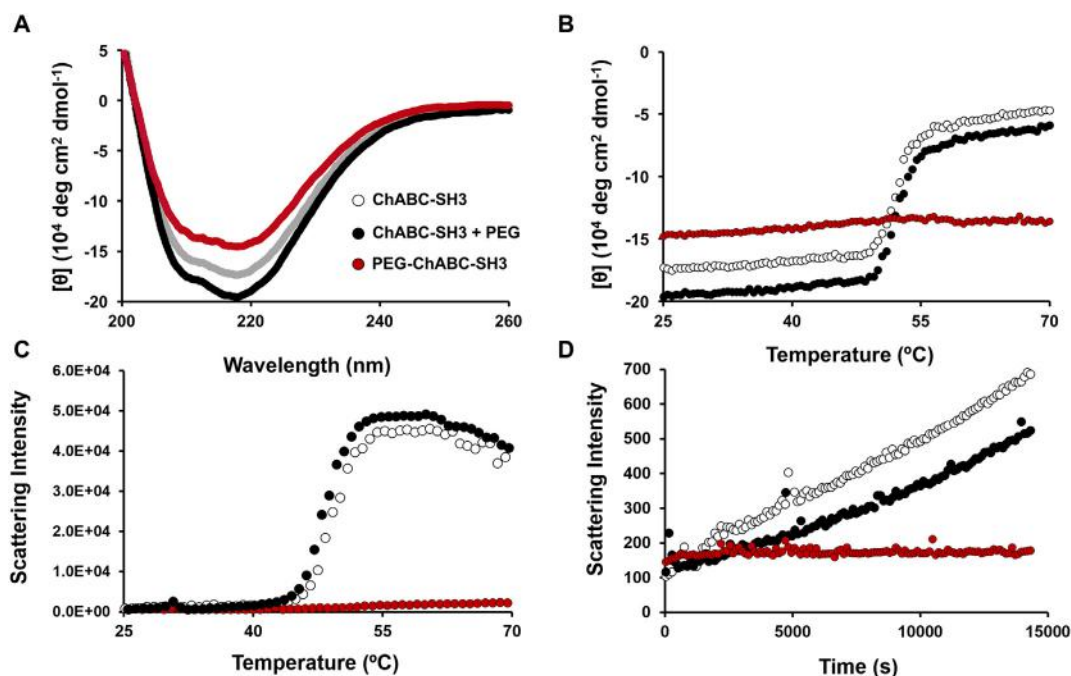


Fig. 5. PEGylation affects ChABC-SH3 unfolding and aggregation. A) Circular dichroism spectra of ChABC-SH3, PEG-ChABC-SH3, and ChABC-SH3 with free PEG from 200 to 260 nm at 25 °C. B) Thermal denaturation curves over 25–70 °C (1 °C/min temperature increase) measured by circular dichroism at 217 nm. C) Thermal denaturation curves over 25–70 °C (1 °C/min temperature increase) measured by scattering intensity of solution. D) Thermal denaturation during incubation at 37 °C for 4 h measured by scattering intensity of solution.

by inhibiting protein unfolding and aggregation, but not through significant structural changes.

3.4. Additive effect of PEGylation and point mutations on chondroitinase ABC-SH3 activity

Since PEGylation and site-directed mutagenesis target complementary pathways to ChABC-SH3 stability and activity, we leveraged the benefits of both in the synthesis of PEG-N1000G-ChABC-SH3. PEG-N1000G-ChABC-SH3 had greater initial ($t = 0$ h) enzymatic activity than ChABC-SH3, PEG-ChABC-SH3, and N1000G-ChABC-SH3 (Fig. 6A). Both N1000G-ChABC-SH3 and PEG-N1000G-ChABC-SH3 also exhibited higher enzymatic activity after 24 and 48 h of incubation at 37 °C (Fig. 6A, B). A combined effect of PEGylation and the point mutation was observed, with the PEG-N1000G-ChABC-SH3 protein demonstrating the highest activity after 48 h and maintaining almost 10 times more activity than the unmodified protein. Both N1000G-ChABC-SH3 and PEG-N1000G-ChABC-SH3 demonstrated a significantly higher AUC and total potential for substrate degradation compared to ChABC-SH3 and PEG-ChABC-SH3 (Fig. 6C). PEG-N1000G-ChABC-SH3 exhibited inhibited protein unfolding and aggregation as had been observed for PEG-ChABC-SH3 and as determined by CD and SLS (Fig. S7).

3.5. Controlled release of PEGylated chondroitinase ABC-SH3 from methylcellulose hydrogels

To determine whether PEGylation and the N1000G point mutation of ChABC-SH3 would affect its release, we compared the *in vitro* release of ChABC-SH3 and PEG-N1000G-ChABC-SH3 from crosslinked methylcellulose hydrogels modified with SH3 binding peptides (MC-peptide, $K_D = 2.7 \times 10^{-5}$ M, 1:100 protein to peptide) and relative to that from crosslinked hydrogels without binding peptides (Fig. 7). We found that PEGylation neither affected the release profile at later timepoints nor the percent protein released; however, it did slow release at 6 h, likely due to the increased molar mass of the PEGylated protein. Significantly more PEG-N1000G-ChABC-SH3 was released from MC

hydrogels lacking binding peptides over the first two days, demonstrating that the affinity between ChABC-SH3 and the SH3 binding peptides was necessary to control protein release.

3.6. *In vivo* degradation of glial scar in stroke-injured brains

Having demonstrated sustained activity and release of PEG-N1000G-ChABC-SH3 *in vitro*, we evaluated its bioactivity in a rat model of stroke. We examined the degradation of the CSPGs of the proteoglycan-rich glial scar that forms following CNS injury after injecting the protein-loaded hydrogels directly onto the epicortex of the brain. The levels of CSPG expression in the lesion and peri-lesional area were compared at 9, 14, and 28 d post-stroke after injection of MC-peptide hydrogels containing PEG-N1000G-ChABC-SH3, ChABC-SH3, or no enzyme. The percentage of CSPG⁺ pixels were quantified in the DAPI⁺ NeuN⁻ cortical lesion and at 100 and 200 μ m distances away from the lesion (*i.e.* the peri-lesion) as depicted (Fig. 8A–D). No differences were observed in lesion sizes (Fig. 8E) or CSPG levels within the cortical lesion between groups and timepoints (Fig. 8F). Interestingly, CSPG levels in the 100 μ m peri-lesion increased significantly over time (9 d vs. 28 d) in the vehicle control group, but not in the ChABC-SH3-treated groups (Fig. 8G). Moreover, animals treated with PEG-N1000G-ChABC-SH3 enzyme exhibited significantly less CSPG expression in the 100 μ m peri-lesion at 14 and 28 d post-stroke compared to the vehicle control (Fig. 8G). Even in the 100–200 μ m peri-lesion, the CSPG levels were significantly reduced with PEG-N1000G-ChABC-SH3 treatment compared to the vehicle at 14 d post stroke (Fig. 8H).

4. Discussion

ChABC is a promising protein therapeutic for treatment following CNS injury, yet its use is largely hindered by its instability and the need for its sustained release due to the continual production of CSPGs over several weeks post-injury [40]. In these studies, we demonstrated that the stability of ChABC can be enhanced through site-directed mutagenesis and PEGylation of exposed lysine residues, leading to reduced

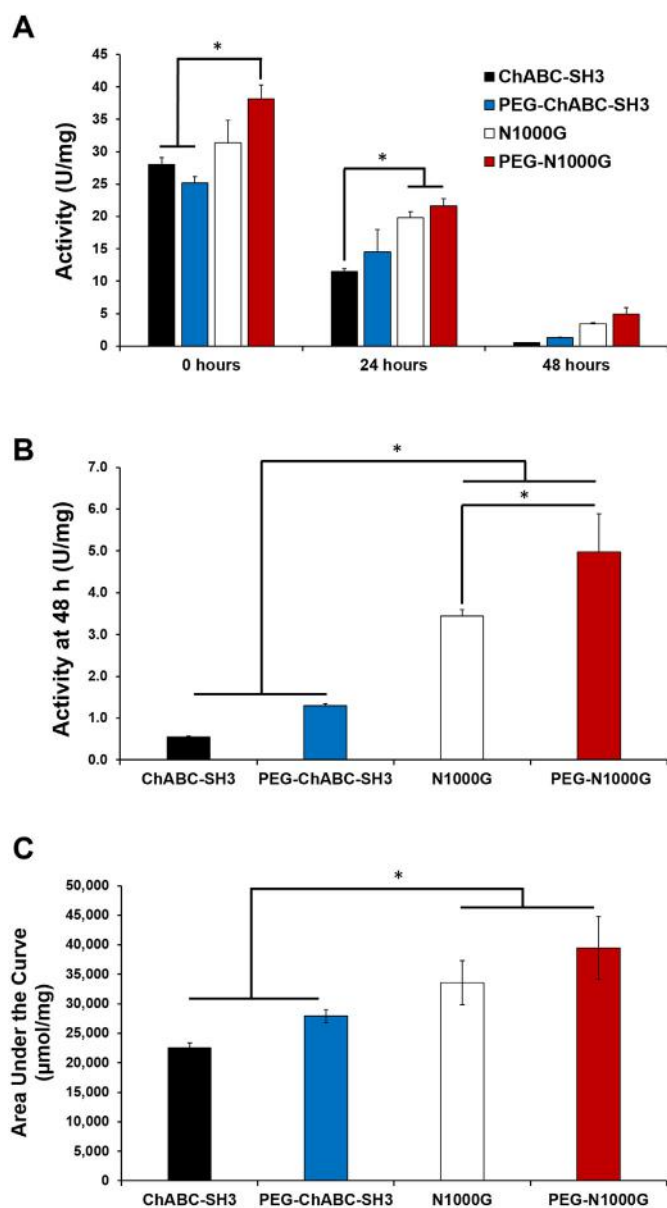


Fig. 6. ChABC-SH3 activity is enhanced with both PEGylation and the N1000G mutation. A) Specific activity of ChABC-SH3, PEG-ChABC-SH3, N1000G-ChABC-SH3, and PEG-N1000G-ChABC-SH3 after incubation in 0.1% BSA in PBS at 37 °C (pH 7.4) for 0, 24, and 48 h. B) Specific activity of ChABC-SH3, PEG-ChABC-SH3, N1000G-ChABC-SH3, and PEG-N1000G-ChABC-SH3 after incubation at 37 °C for 48 h. C) Area under the curve (AUC) or total potential substrate degraded by ChABC-SH3, PEG-ChABC-SH3, N1000G-ChABC-SH3, and PEG-N1000G-ChABC-SH3 over 48 h. ($n = 3$, mean \pm SEM, * $p < .05$).

protein unfolding and aggregation, prolonged enzymatic activity, and increased half-life. We confirmed that we could control the release of this new PEGylated mutant protein, PEG-N1000G-ChABC-SH3, by an affinity mechanism and that its delivery to the brain, 7 d after cortical stroke injury, was effective at reducing CSPG levels in the peri-lesion both 14 and 28 d post-injury compared to delivery of the hydrogel vehicle alone. Interestingly, similar effects were not observed with unmodified ChABC-SH3. These data demonstrate that the improvements observed in ChABC stability and activity *in vitro* translated into increased efficacy *in vivo*.

Site-directed mutagenesis is a valuable tool for investigating the relationship between protein structure and function and can be used to introduce point mutations into a protein sequence to modulate its

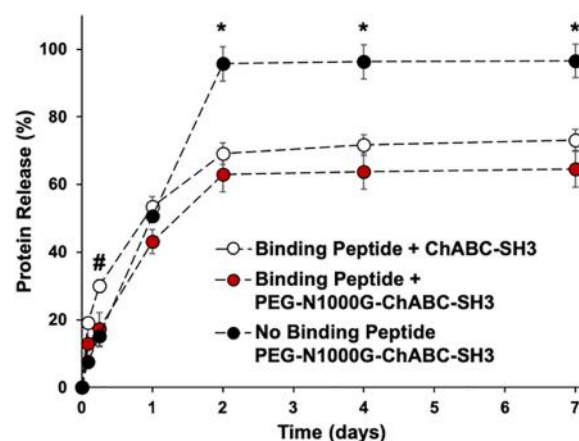


Fig. 7. *In vitro* release of ChABC-SH3 from methylcellulose hydrogels modified with SH3 binding peptides. 20 μg of ChABC-SH3 and PEG-N1000G-ChABC-SH3 were mixed into 100 μL of cross-linked methylcellulose hydrogels with and without binding peptides; hydrogels were allowed to release protein into 400 μL of artificial cerebrospinal fluid over 7 d. Release was plotted as percentage of total protein loaded. ($n = 3$ mean \pm standard error, # $p < .05$ between Binding Peptide + ChABC-SH3 compared to other groups, and * $p < .05$ between No Binding Peptide + PEG-N1000G-ChABC-SH3 compared to other groups at the time points indicated.)

stability and activity. We applied an *in silico* modeling approach to uncover novel stabilizing point mutations in the amino acid sequence of ChABC by using crystal structure information to predict resultant changes in free energy. We experimentally investigated four point mutations based on this approach - N1000G, Q140G, T154F, and S431L; yet, only the N1000G mutation enhanced long-term enzymatic activity, demonstrating the importance of validating *in silico* predictions experimentally. Discrepancies between *in silico* predictions and experimental observations could be due to several reasons. Firstly, our analysis considered the point mutations and truncated sequence of the ChABC domains in the ChABC-SH3 fusion protein compared to the native ChABC crystal structure (1HN0); however, we were unable to model the ChABC and SH3 domains together, due to a lack of crystal structure data, and some estimations were required to model ChABC-SH3 onto the 1HN0 structure. Consequently, the SH3 domain, as well as the additional hexahistidine and FLAG tags on the N and C termini of the protein may have influenced the structure of the ChABC domains unexpectedly, leading to less accurate free energy of mutation predictions. These additional modifications may also explain why the Q140G mutation did not result in the improvements to long-term ChABC activity that have been previously observed by others [14]. Secondly, the protocols used may only be moderately accurate since not all factors affecting protein structure and function can be modeled by Rosetta. Mutations predicted to be stabilizing by the ddG protocol (T154F, S431L), which allowed backbone and sidechain movement, resulted in almost complete loss of enzymatic activity. Thus, we found that the PMutScan protocol, which predicted the N1000G mutation with a fixed backbone, was more appropriate for predicting mutations in ChABC and may warrant further investigation. Lastly, we purposefully chose single point mutations that would not cause large shifts in protein structure, as confirmed by far-UV CD spectra and consistent with other point mutation strategies [12–14]. Since ChABC is a large protein with ~1000 residues, more drastic changes in free energy or combinations of several mutations may be required to stabilize it further.

Since site directed mutagenesis only modestly stabilized ChABC-SH3, we investigated PEGylation as a complementary strategy. PEGylation of therapeutic proteins, which can prevent protein aggregation and increase *in vivo* half-life [20–24], has been explored extensively with proteins of varying sizes, including fibroblast growth factor-2 (18 kDa) [20], epidermal growth factor (6 kDa) [41], and

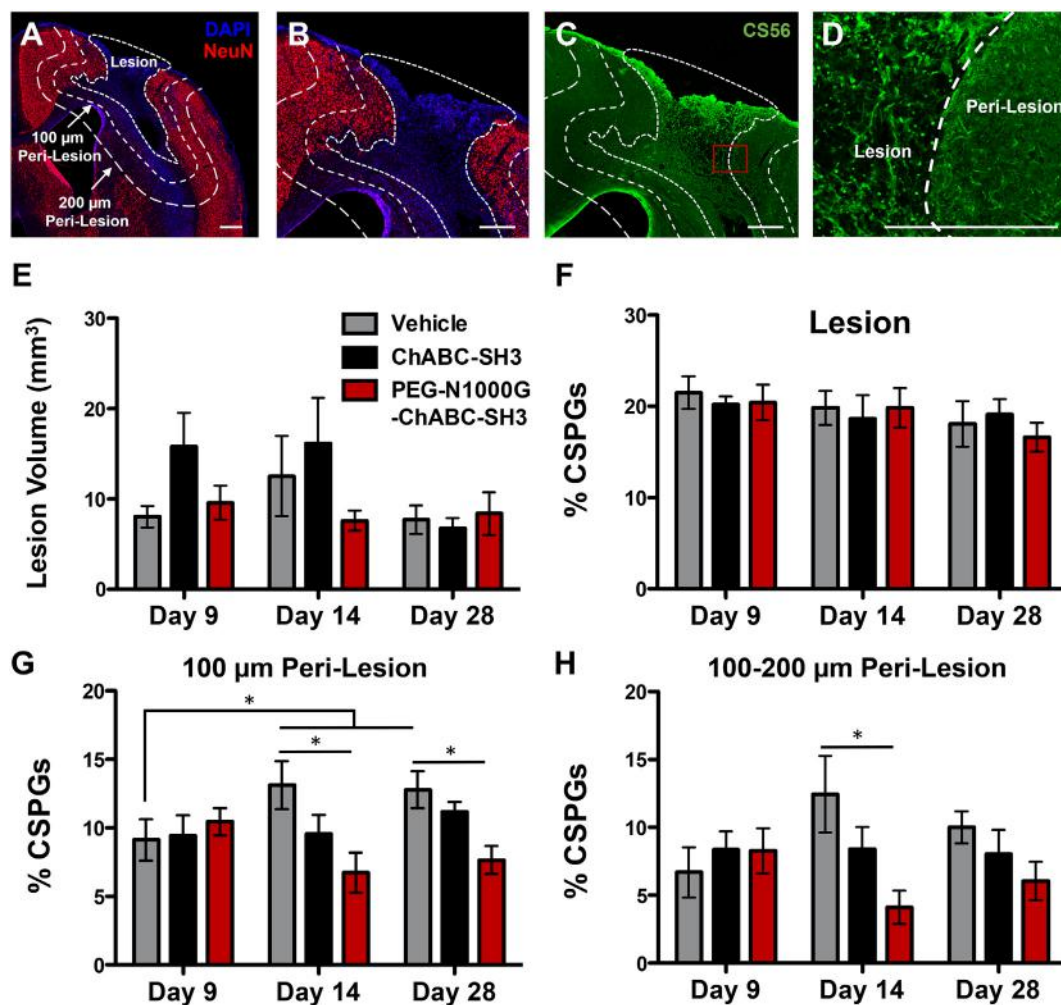


Fig. 8. Effect of ChABC-SH3 and PEG-N1000G-ChABC-SH3 on chondroitin sulfate proteoglycan levels in stroke-injured rat brains. 7 d post-stroke, ChABC-SH3 and PEG-N1000G-ChABC-SH3 were delivered to the cortical surface of the brain in methylcellulose hydrogels containing SH3 binding peptides and compared to vehicle (hydrogel alone). A, B) Representative images of coronal brain sections stained with DAPI (blue) and NeuN (red) to denote lesion (DAPI⁺, NeuN⁻, short dashed line) and 100 μm and 200 μm peri-lesion regions (long dashed lines). C) Chondroitin sulfate proteoglycan staining using CS56 (green) with lesion and peri-lesional regions denoted by dashed lines and area of higher magnification denoted by red box. D) Higher magnification of CS56 staining (green) in lesion and peri-lesional regions (dashed line). (All scale bars = 100 μm) E) Total lesion volume, F) percentage of CS56⁺ pixels compared to total pixel number in the lesion, G) percentage of CS56⁺ pixels compared to total pixel number in the 100 μm peri-lesion, and H) percentage of CS56⁺ pixels compared to total pixel number in the 100–200 μm peri-lesion were measured at 9, 14, and 28 d post-stroke. ($n = 4-5$, mean \pm SEM, * $p < .05$). (For interpretation of the references to colour in this figure legend, the reader is referred to the web version of this article.)

interferon- α (20 kDa) [22], as well as a variety of antibodies (~150 kDa) and antibody fragments (~50 kDa) [21,23]. NHS ester chemistry was chosen for PEGylation in this study due to its ease of use, favorable reaction conditions for preserving ChABC-SH3 bioactivity (1 h at 25 °C, pH 8), and the large number of accessible lysines on the protein. Remarkably, initial ChABC-SH3 activity was not negatively impacted by PEG conjugation, even with up to an average of 12.6 PEG chains per protein, despite the open nature of the catalytic site groove of ChABC. We observed the largest improvement in long-term ChABC-SH3 activity when an average of 6.6–12.6 20-kDa PEG chains were conjugated; this effect is consistent with other reports where protein activity has been improved with PEGylation strategies that employed few, longer (20–40 kDa) PEG chains [21,23]. Covalent conjugation of PEG to ChABC-SH3 was necessary to prevent protein aggregation, which resulted in extended bioactivity. While PEGylation has enhanced tissue penetration of proteins [20], it may also slow release, as we observed *in vitro* with PEG-N1000G-ChABC-SH3 from MC-peptide hydrogels compared to unmodified ChABC-SH3 at an early time point. This effect may be due to diffusion limitations caused by the increased molar mass, increased hydrodynamic radius of the protein, or

entanglement of PEG chains with the methylcellulose polymer. Importantly, we confirmed that PEGylation of N1000G-ChABC-SH3 did not interfere with the SH3-binding peptide interaction in the methylcellulose hydrogels, and its sustained release over 7 days was similar to that of unmodified ChABC-SH3.

The tissue effects of PEG-N1000G-ChABC-SH3 were compared to those of ChABC-SH3 and vehicle controls in an endothelin-1 rat model of stroke. The endothelin-1 model is a well-established model of moderate, clinical stroke [42] and, at 7 d after injury, the glial scar has evolved enough that beneficial effects of ChABC on the glial scar / CSPG levels should be evident [40,43–45]. While no differences in lesion volume were observed between treatment groups, these results corroborate other studies that report no effect of ChABC treatment on stroke or spinal cord lesion size [46–49]. CSPG expression in the peri-lesion, specifically up to 200 μm away from the lesion border, was significantly reduced at 14 and 28 d post-injury with PEG-N1000G-ChABC-SH3 treatment vs. ChABC-SH3 and vehicle treatments. We attributed greater proteoglycan degradation of PEG-N1000G-ChABC-SH3 to increased long-term bioactivity, decreased aggregation, and shielding from cellular uptake. When treated with vehicle alone, CSPG

expression in the peri-lesion continued to increase over 14–28 d post-stroke, which is consistent with other models [40], thereby validating our injury model. Differences in CSPG expression were not observed at the earliest time point of analysis (9 d after injury or 2 d after hydrogel injection), likely because insufficient concentrations of ChABC had reached the peri-lesional tissue [49]. We demonstrate a significant reduction in CSPG levels for at least 3 weeks after PEG-N1000G-ChABC-SH3 administration, which corresponds with the time period of peak CSPG production [40] and is longer than what has been previously achieved with sustained delivery [48,49]. Interestingly, CSPG expression within the lesion itself appeared to be neither impacted by PEG-N1000G-ChABC-SH3 nor ChABC-SH3 treatment. This may be due to the dynamic nature of the stroke injury site, in which CSPGs are continually produced by inflammatory cells and reactive astrocytes at a higher rate in the lesion than in the surrounding penumbra and undamaged tissue, thereby leading to CSPGs digested by ChABC being more quickly replaced in the lesion. Moreover, CSPG production involves shuttling the material through intracellular vesicles prior to secretion into the extracellular matrix, and during this process, intracellular CSPGs are inaccessible to ChABC [50]. Thus, in areas of high CSPG turnover (*i.e.* the stroke injury site), higher quantities of vesicle-bound CSPGs, which cannot be digested by ChABC, may exist. Finally, ChABC has been shown to degrade different subtypes of CSPGs with varying levels of efficacy; since different CSPGs are deposited in and around the stroke lesion site [40,51], CSPGs surrounding the lesion may be more sensitive to ChABC digestion than those produced within the lesion.

Changes in CSPG distribution along the lesion boundary are especially promising for tissue and functional recovery following CNS injury, enabling local plasticity and axonal growth into damaged tissue to re-establish lost neuronal connections due to glial scar and/or perineuronal net degradation [47]. Carmichael and colleagues identified a second zone of increased axonal sprouting and growth-promoting gene expression adjacent to the growth-inhibitory peri-lesional tissue (0.5–2 mm from the stroke infarct) that may engage in plastic rearrangement following injury [40]. This zone is a likely source of axonal outgrowth into damaged tissue following removal of inhibitory extracellular matrix cues by ChABC. ChABC delivery alone often results in modest behavioral recovery [9,49], thereby underscoring the need for co-delivery with a neurotrophic biomolecule or cell source that can readily target tissue that has been primed for repair by ChABC-mediated proteoglycan degradation. Since CSPG deposition peaks between 7 and 14 days after the initial injury in the stroke lesion area [40], subacute delivery of ChABC (*i.e.* 7 days post-stroke) that enables sustained activity of the enzyme for 1–2 weeks ensures that the early protective effects of the glial scar are maintained while the later inhibitory cues are reduced [44]. Thus, early and sustained delivery of ChABC should promote tissue plasticity that can be then be further harnessed with regenerative cues. Early and sustained delivery of ChABC should promote tissue plasticity that can be then be further harnessed with regenerative cues.

5. Conclusions

We employed a powerful computational approach to investigate point mutations in ChABC that allowed screening of over 20,000 mutations *in silico*, 4 of which were screened *in vitro* and one of which significantly improved *in vitro* activity. PEGylation further enhanced the stability of this fragile enzyme, resulting in increased degradation of the proteoglycan component of the glial scar in a rat model of stroke injury and significantly reduced CSPG expression levels up to 28 d post-injury. Thus, we demonstrated, for the first time, PEGylation of ChABC and its consequent improved long-term efficacy *in vivo*. Combined with our sustained release platform, this improved ChABC variant has great potential as a viable therapeutic for CNS repair in the future.

Acknowledgements

We thank Dr. Ricky Siu for his assistance performing stroke injury surgeries and sectioning tissue, Dr. Vianney Delplace for material synthesis, and Dr. Walid Houry for the use of his circular dichroism spectrophotometer. We also thank Dr. Brian Shoichet (University of California – San Francisco) and Greg Wasney (Sickkids Structural and Biophysical Core Facility) for helpful discussions and advice. We are grateful for funding provided by the Canadian Institutes of Health Research (Foundation Grant to MSS), Natural Sciences and Engineering Research Council of Canada (Discovery Grant to MSS, Post-doctoral Fellowship to MHH), and Canada First Research Excellence Fund Medicine by Design to the University of Toronto (to MSS). Finally, we thank members of the Shoichet lab for thoughtful review of this manuscript.

Appendix A. Supplementary data

Supplementary data to this article can be found online at <https://doi.org/10.1016/j.jconrel.2019.01.033>.

References

- [1] M.H. Hettiaratchi, T. Führmann, M.S. Shoichet, Recent advances in regenerative medicine approaches for spinal cord injuries, *Curr. Opin. Biomed. Eng.* 4 (2017) 40–49.
- [2] A. Tuladhar, S.L. Payne, M.S. Shoichet, Harnessing the potential of biomaterials for brain repair after stroke, *Front. Mater.* 5 (2018) 14.
- [3] N. Harris, S. Carmichael, D. Hovda, R. Sutton, Traumatic brain injury results in disparate regions of chondroitin sulfate proteoglycan expression that are temporally limited, *J. Neurosci. Res.* 87 (2009) 2937–2950.
- [4] L.L. Jones, R.U. Margolis, M.H. Tuszynski, The chondroitin sulfate proteoglycans neurocan, brevican, phosphacan, and versican are differentially regulated following spinal cord injury, *Exp. Neurol.* 182 (2003) 399–411.
- [5] C.M. Galtrey, J.W. Fawcett, The role of chondroitin sulfate proteoglycans in regeneration and plasticity in the central nervous system, *Brain Res. Rev.* 54 (2007) 1–18.
- [6] T.S. Wilems, S.E. Sakiyama-Elbert, Sustained dual drug delivery of anti-inhibitory molecules for treatment of spinal cord injury, *J. Control. Release* 213 (2015) 103–111.
- [7] N.J. Tester, A.H. Plaas, D.R. Howland, Effect of body temperature on chondroitinase ABC's ability to cleave chondroitin sulfate glycosaminoglycans, *J. Neurosci. Res.* 85 (2007) 1110–1118.
- [8] S.A. Shirdel, K. Khalifeh, A. Golestani, B. Ranjbar, K. Khajeh, Critical role of a loop at C-terminal domain on the conformational stability and catalytic efficiency of chondroitinase ABC I, *Mol. Biotechnol.* 57 (2015) 727–734.
- [9] J.J. Hill, K. Jin, X.O. Mao, L. Xie, D.A. Greenberg, Intracerebral chondroitinase ABC and heparan sulfate proteoglycan glypican improve outcome from chronic stroke in rats, *Proc. Natl. Acad. Sci.* 109 (2012) 9155–9160.
- [10] E.J. Bradbury, L.D. Moon, R.J. Popat, V.R. King, G.S. Bennett, P.N. Patel, et al., Chondroitinase ABC promotes functional recovery after spinal cord injury, *Nature* 416 (2002) 636–640.
- [11] L.D. Moon, R.A. Asher, K.E. Rhodes, J.W. Fawcett, Regeneration of CNS axons back to their target following treatment of adult rat brain with chondroitinase ABC, *Nat. Neurosci.* 4 (2001) 465–466.
- [12] M.E. Shahabuddin, K. Khajeh, M. Maleki, A. Golestani, Improvement of activity and stability of Chondroitinase ABC I by introducing an aromatic cluster at the surface of protein, *Enzym. Microb. Technol.* 105 (2017) 38–44.
- [13] A. Kheirollahi, K. Khajeh, A. Golestani, Rigidifying flexible sites: an approach to improve stability of chondroitinase ABC I, *Int. J. Biol. Macromol.* 97 (2017) 270–278.
- [14] M. Nazari-Robati, K. Khajeh, M. Aminian, N. Mollania, A. Golestani, Enhancement of thermal stability of chondroitinase ABC I by site-directed mutagenesis: an insight from Ramachandran plot, *Biochim. Biophys. Acta* 1834 (2013) 479–486.
- [15] H. Lee, R.J. McKeon, R.V. Bellamkonda, Sustained delivery of thermostabilized chABC enhances axonal sprouting and functional recovery after spinal cord injury, *Proc. Natl. Acad. Sci.* 107 (2009) 3340–3345 (pnas.0905437106).
- [16] M. Nazari-Robati, K. Khajeh, M. Aminian, M. Fathi-Roudsari, A. Golestani, Co-solvent mediated thermal stabilization of chondroitinase ABC I form *Proteus vulgaris*, *Int. J. Biol. Macromol.* 50 (2012) 487–492.
- [17] A. Raspa, E. Bolla, C. Cuscona, F. Gelain, Feasible stabilization of chondroitinase ABC enables reduced astrogliosis in a chronic model of spinal cord injury, *CNS Neurosci. Ther.* 25 (2018) 86–100.
- [18] C.S. Fishburn, The pharmacology of PEGylation: balancing PD with PK to generate novel therapeutics, *J. Pharm. Sci.* 97 (2008) 4167–4183.
- [19] W. Huang, V. Lunin, Y. Li, S. Suzuki, N. Sugiura, H. Miyazono, et al., Crystal structure of *Proteus vulgaris* chondroitin sulfate ABC lyase I at 1.9 Å resolution, *J. Mol. Biol.* 328 (2003) 623–634.
- [20] C.E. Kang, C.H. Tator, M.S. Shoichet, Poly (ethylene glycol) modification enhances

- penetration of fibroblast growth factor 2 to injured spinal cord tissue from an intrathecal delivery system, *J. Control. Release* 144 (2010) 25–31.
- [21] L.S. Lee, C. Conover, C. Shi, M. Whitlow, D. Filpula, Prolonged circulating lives of single-chain Fv proteins conjugated with polyethylene glycol: a comparison of conjugation chemistries and compounds, *Bioconjug. Chem.* 10 (1999) 973–981.
- [22] P. Bailon, C.-Y. Won, PEG-modified biopharmaceuticals, *Expert Opin. Drug Deliv.* Vol. 6 (2009) 1–16.
- [23] A.P. Chapman, PEGylated antibodies and antibody fragments for improved therapy: a review, *Adv. Drug Deliv. Rev.* Vol. 54 (2002) 531–545.
- [24] R.S. Rajan, T. Li, M. Aras, C. Sloey, W. Sutherland, H. Arai, et al., Modulation of protein aggregation by polyethylene glycol conjugation: GCSF as a case study, *Protein Sci.* 15 (2006) 1063–1075.
- [25] K. Vulic, M.S. Shoichet, Tunable growth factor delivery from injectable hydrogels for tissue engineering, *J. Am. Chem. Soc.* 134 (2011) 882–885.
- [26] R.D. Finn, P. Coghill, R.Y. Eberhardt, S.R. Eddy, J. Mistry, A.L. Mitchell, et al., The Pfam protein families database: towards a more sustainable future, *Nucleic Acids Res.* 44 (2015) D279–D285.
- [27] Database P. Protein: CABCI_PROVU (P59807). Pfam Database.
- [28] R.F. Alford, A. Leaver-Fay, J.R. Jeliazkov, M.J. O'Meara, F.P. DiMaio, H. Park, et al., The Rosetta all-atom energy function for macromolecular modeling and design, *J. Chem. Theory Comput.* 13 (2017) 3031–3048.
- [29] F. Richter, I. Fonfara, B. Bouazza, C.H. Schumacher, M. Bratovič, E. Charpentier, et al., Engineering of temperature-and light-switchable Cas9 variants, *Nucleic Acids Res.* 44 (2013) gkw930.
- [30] H. Park, P. Bradley, P. Greisen Jr., Y. Liu, V.K. Mulligan, D.E. Kim, et al., Simultaneous optimization of biomolecular energy functions on features from small molecules and macromolecules, *J. Chem. Theory Comput.* 12 (2016) 6201–6212.
- [31] M.M. Pakulska, K. Vulic, M.S. Shoichet, Affinity-based release of chondroitinase ABC from a modified methylcellulose hydrogel, *J. Control. Release* 171 (2013) 11–16.
- [32] L. Whitmore, B. Wallace, DICHROWEB, an online server for protein secondary structure analyses from circular dichroism spectroscopic data, *Nucleic Acids Res.* 32 (2004) W668–W673.
- [33] M.M. Pakulska, K. Vulic, R.Y. Tam, M.S. Shoichet, Hybrid crosslinked methylcellulose hydrogel: a predictable and tunable platform for local drug delivery, *Adv. Mater.* 27 (2015) 5002–5008.
- [34] A. Tuladhar, C.M. Morshead, M.S. Shoichet, Circumventing the blood–brain barrier: local delivery of cyclosporin a stimulates stem cells in stroke-injured rat brain, *J. Control. Release* 215 (2015) 1–11.
- [35] H.C. Abeysinghe, L. Bokhari, A. Quigley, M. Choolani, J. Chan, G.J. Dusing, et al., Pre-differentiation of human neural stem cells into GABAergic neurons prior to transplant results in greater repopulation of the damaged brain and accelerates functional recovery after transient ischemic stroke, *Stem Cell Res. Ther.* 6 (2015) 186.
- [36] N. Otsu, A threshold selection method from gray-level histograms, *IEEE Trans. Syst. Man Cyber.* 9 (1979) 62–66.
- [37] W.-H. Tsai, Moment-preserving Thresholding: A New Approach, in: O.G. Lawrence, K. Rangachar (Eds.), *Document Image Analysis*, IEEE Computer Society Press, 1995, pp. 44–60.
- [38] V. Prabhakar, R. Raman, I. Capila, C.J. Bosques, K. Pojasek, R. Sasisekharan, Biochemical characterization of the chondroitinase ABC I active site, *Biochem. J.* 390 (2005) 395–405.
- [39] L. Schrödinger, The PyMOL Molecular Graphics System, Version 1.4, (2010).
- [40] S.T. Carmichael, I. Archibeque, L. Luke, T. Nolan, J. Momiy, S. Li, Growth-associated gene expression after stroke: evidence for a growth-promoting region in perinfarct cortex, *Exp. Neurol.* 193 (2005) 291–311.
- [41] Y. Wang, M.J. Cooke, N. Sachewsky, C.M. Morshead, M.S. Shoichet, Bioengineered sequential growth factor delivery stimulates brain tissue regeneration after stroke, *J. Control. Release* 172 (2013) 1–11.
- [42] V. Windle, A. Szymanska, S. Granter-Button, C. White, R. Buist, J. Peeling, et al., An analysis of four different methods of producing focal cerebral ischemia with endothelin-1 in the rat, *Exp. Neurol.* 201 (2006) 324–334.
- [43] A. Rolls, R. Shechter, M. Schwartz, The bright side of the glial scar in CNS repair, *Nat. Rev. Neurosci.* 10 (2009) 235.
- [44] M.A. Anderson, J.E. Burda, Y. Ren, Y. Ao, T.M. O'Shea, R. Kawaguchi, et al., Astrocyte scar formation aids central nervous system axon regeneration, *Nature* 532 (2016) 195.
- [45] Z. Liu, Y. Li, Y. Cui, C. Roberts, M. Lu, U. Wilhelmsson, et al., Beneficial effects of GFAP/vimentin reactive astrocytes for axonal remodeling and motor behavioral recovery in mice after stroke, *Glia* 62 (2014) 2022–2033.
- [46] L. Gherardini, M. Gennaro, T. Pizzorusso, Perilesional treatment with chondroitinase ABC and motor training promote functional recovery after stroke in rats, *Cereb. Cortex* 25 (2013) 202–212.
- [47] S. Soleman, P.K. Yip, D.A. Duricki, L.D. Moon, Delayed treatment with chondroitinase ABC promotes sensorimotor recovery and plasticity after stroke in aged rats, *Brain* 135 (2012) 1210–1223.
- [48] T. Führmann, P. Anandakumaran, S. Payne, M. Pakulska, B.V. Varga, A. Nagy, et al., Combined delivery of chondroitinase ABC and human induced pluripotent stem cell-derived neuroepithelial cells promote tissue repair in an animal model of spinal cord injury, *Biomed. Mater.* 13 (2017) 024103.
- [49] M.M. Pakulska, C.H. Tator, M.S. Shoichet, Local delivery of chondroitinase ABC with or without stromal cell-derived factor 1 α promotes functional repair in the injured rat spinal cord, *Biomaterials* 134 (2017) 13–21.
- [50] R. Lin, J.C. Kwok, D. Crespo, J.W. Fawcett, Chondroitinase ABC has a long-lasting effect on chondroitin sulphate glycosaminoglycan content in the injured rat brain, *J. Neurochem.* 104 (2008) 400–408.
- [51] J.R. Siebert, A. Conta Steencken, D.J. Osterhout, Chondroitin sulfate proteoglycans in the nervous system: inhibitors to repair, *Biomed. Res. Int.* (2014) 845323.